Preliminary Study of a Novel R718 Compression Refrigeration Cycle Using a Three-Port Condensing Wave Rotor

Amir A. Kharazi
e-mail: kharazia@egr.msu.edu

Pezhman Akbari
e-mail: akbari@egr.msu.edu

Norbert Müller
e-mail: mueller@egr.msu.edu

Department of Mechanical Engineering
Michigan State University,
East Lansing, MI 48824-1226

Using a novel 3-port condensing wave rotor enhancing the turbocompression in a R718 refrigeration cycle, which uses only water as a refrigerant, has been introduced. The wave-rotor implementation can increase efficiency and reduce size and cost of R718 units. The condensing wave rotor employs pressurized water to pressurize, desuperheat, and condense the refrigerant vapor—all in one dynamic process. The underlying phenomena of flash evaporation, shock wave compression, desuperheating, and condensation inside the wave rotor channels are described in a wave and phase-change diagram. The thermodynamic process is shown in pressure–enthalpy and temperature–entropy diagrams. A computer program based on a thermodynamic model was generated to evaluate the performance of R718 baseline and wave-rotor-enhanced cycles. The effect of some key parameters on the performance enhancement is demonstrated as an aid for optimization. A performance map summarizes the findings. It shows optimum wave rotor pressure ratio and maximum relative performance improvement of R718 cycles by using the 3-port condensing wave rotor. [DOI: 10.1115/1.1850503]

Introduction

The potential for using wave devices in thermodynamic cycles for power generation, propulsion, and refrigeration has attracted the attention of researchers since the early twentieth century. Shock tubes, shock tunnels, pressure exchangers, pulse combustors, pulse detonation engines, and wave rotors are among the best-known wave devices developed so far. These devices represent applications of classical nonsteady one-dimensional compressible flow theory. It is well known, but not yet widely employed, that time-dependent flow devices can generate much greater pressure rises than those obtained in steady-state flow devices [1–3]. By generating shock waves in appropriate geometries, unsteady wave machines can transfer the energy of a high-pressure fluid directly to another low-pressure fluid without using mechanical components such as pistons or vaned impellers.

Within the family of wave devices, wave rotors have demonstrated an attractive potential for reaching the ultrahigh performance targets of power systems and for lowering their cost. Considerable amount of research has been devoted to the progress and development of wave rotor technology, especially in the past few decades. Most of the work in the U.S. expands from the early efforts of the General Electric Company (GE), General Power Corporation (GPC), and Rolls Royce [4,5] to the recent activities of the wave rotor team at NASA Glenn Research Center (GRC) collaborated by the U.S. Army Research Laboratory (ARL) and Rolls-Royce Allison [6–14].

In a gas turbine, a wave rotor provides a pressure gain additional to that provided by the compressor. It also enables a higher cycle peak temperature without raising the turbine inlet temperature. This is because a part of the energy of the burned gas leaving the combustion chamber is used in a shock compression process to increase the pressure and temperature of the fresh air before it enters the combustion chamber. Therefore, a wave rotor enhances significantly the performance of a gas turbine engine by increasing both the output work and overall thermal efficiency, hence reducing the specific fuel consumption considerably [15–17]. Detailed descriptions of wave rotor operations and configurations are provided in the references cited above and are not repeated here.

The application of wave rotors is not limited to gas turbine engines. Brown Boveri Company (BBC) in Switzerland, later known as Asea Brown Boveri (ABB), has a long history of using wave rotors as superchargers in passenger car and heavy diesel engines [18–26]. ABB's pressure wave supercharger termed as the Comprex® has been used commercially in several passenger car engines in the past three decades.

Wave rotors also have been used for air-cycle refrigeration systems [27–29]. Power Jets Ltd in the U.K. utilized wave rotor technology in the design and development of two prototype air-cycle refrigerators used for environmental cooling purposes. The prototypes were installed and employed in gold mines in India and South Africa and performed the same duty as equivalent vapor-cycle machines, but with lower weight and bulk.

The present study demonstrates the performance improvement of a turbo-compression refrigeration cycle that uses water as refrigerant (R718) by utilizing a novel 3-port condensing wave rotor. The phase change of the fluid inside the wave rotor channels in a R718 refrigeration application is a major difference when compare to the operation of a wave rotor in a gas turbine cycle or an air refrigeration cycle. Furthermore, the high-pressure fluid used to compress the low-pressure fluid is at lower temperature [3]. Adding a wave rotor to a R718 cycle enables a greater temperature lift or reduces the compressor pressure ratio which is crucial for the R718 chiller technology, where the stage pressure ratio is very much limited by the thermodynamic properties of water vapor. Some structural and economic advantages of integrating both 4-port and 3-port wave rotors in a R718 cycle have been discussed in a previous study [3]. Utilizing a 3-port wave rotor appears more promising because it combines the function of a compressor stage and the condenser in one compact unit. Both pressure rise and condensation occur inside the wave rotor channels.

Contributed by the International Gas Turbine Institute (IGTI) of THE AMERICAN SOCIETY OF MECHANICAL ENGINEERS for publication in the ASME JOURNAL OF ENGINEERING FOR GAS TURBINES AND POWER. Paper presented at the International Gas Turbine and Aeroengine Congress and Exhibition, Vienna, Austria, June 13–17, 2004, Paper No. 2004-GT-53622. Manuscript received by IGTI, October 1, 2003; final revision, March 1, 2004. IGTI Review Chair: A. J. Strazisar.

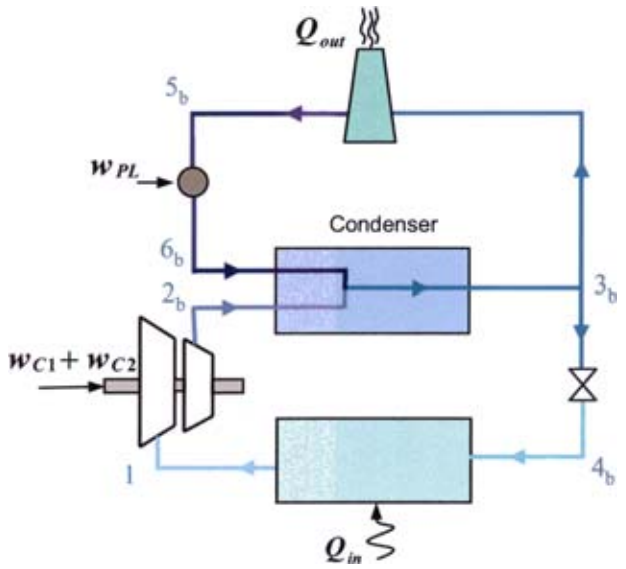

Fig. 1 Schematic of an R718 cycle with direct condensation and evaporation

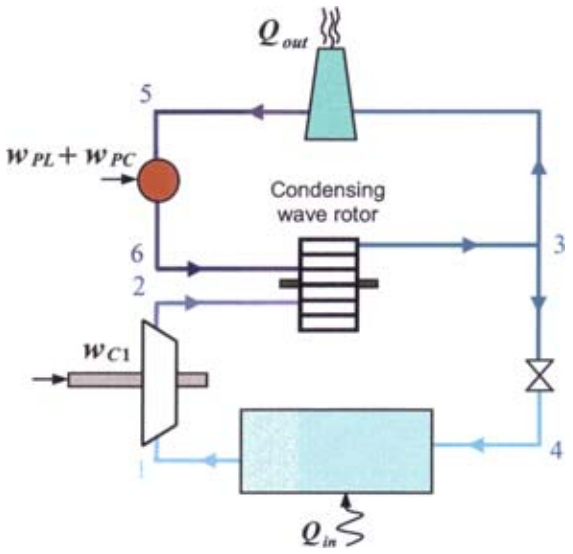

Fig. 2 Schematic of an R718 cycle enhanced by a 3-port condensing wave rotor substituting for the condenser and one compressor stage

Water as a Refrigerant

Water is a natural and clean refrigerant with no Ozone Depletion Potential (ODP=0), no contribution to the global warming (GWP=0), and without any safety risk. It is chemically stable, nontoxic, nonflammable, commonly available, and easily disposable after use. In R718 systems, water serves as both refrigerant and heat transfer fluid. Therefore, direct heat exchangers can be used for evaporator and condenser increasing the energy-saving potential. Moreover, water can function as a working fluid for refrigeration and heat pump cycles in the range of evaporation temperature of 0°C to very high temperatures (e.g., 150°C) [30–33]. Figure 1 depicts schematically a R718 cycle with direct condenser and direct evaporator.

There are a few fundamental differences between water and traditional refrigerants. At the triple point, the vapor pressure of water is only 611 Pa, which is less than 1% of the atmospheric pressure. The low operating pressures of water-vapor refrigeration systems combined with the steep vapor pressure curve of water requires compression systems that can handle large-volume flows and deliver high-pressure ratios [34–36]. This states challenges for the compressor design. While single stage turbocompressors commonly deliver large-volume flows with mostly insufficient pressure ratios, positive displacement compressors can obtain high-pressure ratios but only for relative small-volume flows. A possible compromise is the use of multistage turbocompressors with intercooler. However, this is expensive and bulky. The presented work is part of the ongoing research to improve the compressors, heat exchangers, and to reduce the size of the whole units. Any improvement in compressor and heat exchanger technology has a direct effect on the cost and efficiency of the R718 units.

R-718 Refrigeration Cycle Enhanced With a 3-Port Condensing Wave Rotor

Using a 3-port condensing wave rotor in a water refrigeration cycle appears as a promising technology. It can improve the coefficient of performance (COP) of R718 units while reducing their cost and size. Its successful implementation may substitute three subsystems: the intercooler, one compressor stage, and the condenser.

Figure 2 shows a schematic of a R718 cycle using a 3-port condensing wave rotor. A schematic design of a condensing wave rotor is depicted in Fig. 3. In this innovative design, condensation of vapor happens inside the wave rotor channels as explained below and depicted in Figs. 4 and 5. Figure 4 schematically shows a model for the condensation process inside a channel of a 3-port condensing wave rotor. Figure 5 shows a corresponding schematic wave and phase-change diagram.

Coming from the turbocompressor (2), the superheated vapor flows continuously through a vapor collector (Fig. 3) to the inlet port of the wave rotor located at one of the two stationary end plates. By rotating the wave rotor between the two end plates, the wave rotor channels are opened to the port and filled with the incoming water vapor. The region (*a*) in Figs. 4 and 5 is the state

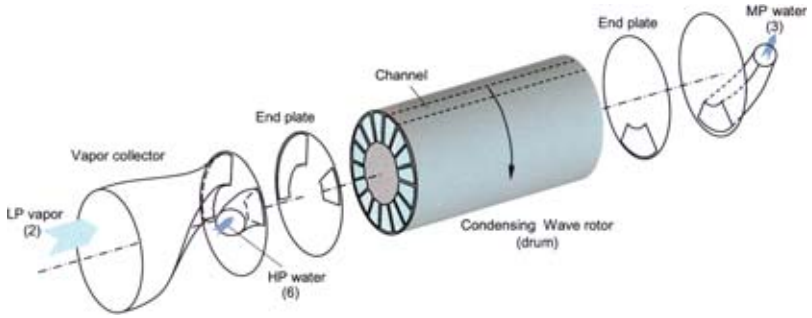

Fig. 3 Schematic of a 3-port condensing wave rotor

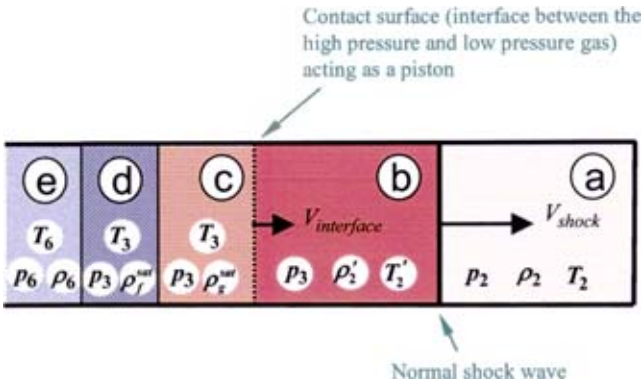

Fig. 4 Regions modeled for each channel during shock compression and condensation

after the filling process is completed. After further rotation, the channels meet the second-inlet port (6) through which the high-pressure low-temperature water (*e*) comes in and is exposed to the low-pressure high-temperature superheated vapor in region (*a*). Due to the sudden pressure drop (from p_6 to p_2), all the heat cannot be contained in the incoming water as sensible heat and the heat surplus is transformed into latent heat of vaporization. It is the so-called flash evaporation or flashing phenomenon [37,38]. Therefore, one portion of the incoming water suddenly vaporizes (*c*) and the remaining part cools down (*d*). The frontal area of the saturated vapor generated by the flash evaporation (*c*) is called *contact interface* and acts like a fast moving piston. It causes a shock wave triggered from the leading edge of the inlet port traveling through the superheated low-pressure vapor which exists inside the channel (*a*). The shock wave travels with supersonic speed (V_{shock}) faster than the contact interface ($V_{interface}$). Therefore, the trajectory of the shock wave (solid line in Fig. 5) has a smaller slope than the incoming water and the contact interface of the generated vapor (dashed line in Fig. 5). Behind the moving shock wave (*b*) the temperature is increased from T_2 to $T_{2'}$ and the pressure is increased from p_2 to $p_{2'}=p_3$ due to the shock compression. The latter is a design decision similar to a tuning condition. With it, the pressure at the inlet port (p_6) is set to an appropriate value that generates the pressure ratio p_6/p_2 required to trigger the desired shock wave. The shock wave increases the pressure of the superheated vapor from p_2 to p_3 at which the vapor will be condensed. This shows that the fluid in its liquid

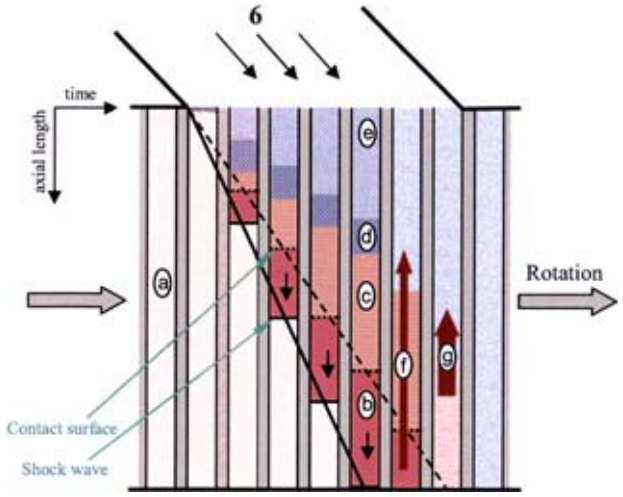

Fig. 5 Schematic wave and phase-change diagram for the 3-port condensing wave rotor (high-pressure part)

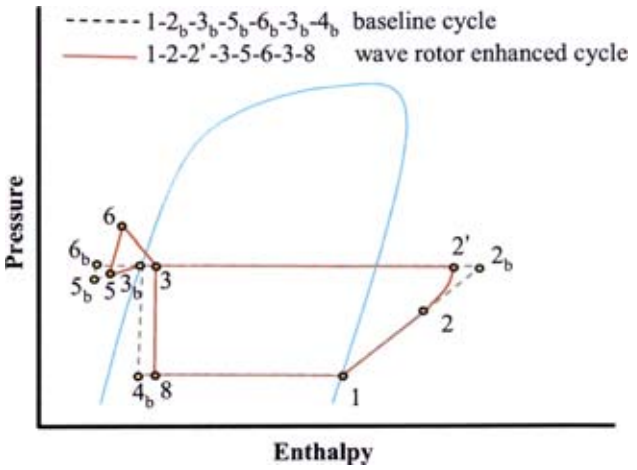

Fig. 6 Schematic *p–h* diagram of an R718 baseline cycle and enhanced cycle with a 3-port condensing wave rotor

state serves as a ''work capacitor'' storing pump work to release it during its expansion in the wave rotor channels for the simultaneous vapor compression. Therefore, in the enhanced system the pump in the cooling water cycle not only has to provide the work necessary to overcome the pressure loss in the heat rejecter cycle (w_{PL}) but also the work necessary for the shock wave compression in the wave rotor channels (w_{PC}). The pressure behind the shock wave (*b*) is imposed on the vapor generated by the flash evaporation (*c*). It is the pressure at the water surface and the equilibrium pressure at which the evaporation decays $p(c)=p(b)=p_3$. Hence, both generated vapor and the cooled water obtain saturation temperature $T_3=T_{sat}(p_3)$.

Due to the contact of the superheated compressed vapor (*b*) with the cold incoming water, the superheated vapor is desuperheated and its heat is transferred (*f*) to the incoming water. This continues until the equilibrium temperature T_3 is achieved in region (*b*) and the superheated vapor is changed to saturated vapor. Subsequently, the incoming water compresses the saturated vapor further and condenses it, while the latent heat is transferred to the incoming water (*g*). The water, which is nearly a fully condensed two-phase vapor with a typical quality of 0.005, is scavenged through the only outlet of the wave rotor (3). The scavenging process may be supported by gravity and pump power.

The schematic pressure–enthalpy ($p-h$) and temperature–entropy ($T-s$) diagrams of both the baseline and the wave-rotor-enhanced cycle are depicted in Figs. 6 and 7, respectively. Both cycles start at the outlet of the evaporator 1, where the vapor is saturated. Point 2_b represents the compressor outlet of the baseline cycle whereas point 2 is the compressor outlet of the wave-rotor-enhanced cycle that allows using a compressor with a lower pressure ratio. 2′ is an intermediate point inside the wave rotor channels that corresponds to the flow properties in region (*b*) right after the shock wave. The slope between points 2 and 2′ is greater than that between points 1 and 2_b because the shock compression typically happens with a higher efficiency [1–3]. Still inside the wave rotor channel, the superheated vapor is desuperheated to the equilibrium temperature $T_3(2'\rightarrow 3)$. State 3 is actually much closer to the liquid region than shown in Figs. 6 and 7 since the mass flow rate of the cooling water cycle is much greater than that of the refrigerant cycle. Knowing about this, it becomes also clear that the distances between points 3, 5, and 6 are exaggerated in both diagrams. The expansion process (6→3) releases the energy consumed by the compression process of the vapor (2→2′) all within the wave rotor channels. Coming from the only outlet port of the wave rotor (3), the flow diverges. The small fraction used as refrigerant is directed to the expansion valve and is expanded in a constant enthalpy process (3→4), while the most part of flow out

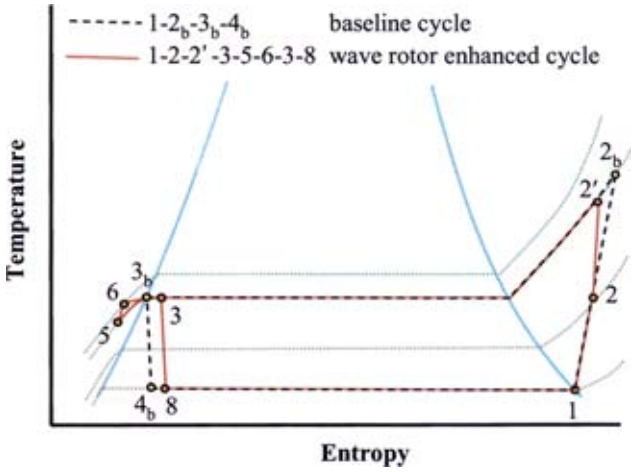

Fig. 7 Schematic *p–h* diagram of an R718 baseline cycle (cooling water cycle not shown) and enhanced cycle with a 3-port condensing wave rotor

of the wave rotor goes to the heat rejecter (cooling tower or similar) where it cools off (3→5). Afterwards the pressure is again increased (5→6) by the pump, providing the energy for the vapor compression in the wave rotor (w_{PC}) and compensating the pressure loss in the heat rejecter and piping (w_{PL}).

Performance Evaluation

A computer code based on the thermodynamic model described above was generated for performance evaluation of R718 refrigeration cycles enhanced with 3-port condensing wave rotors. The evaporator temperature (T_1) and heat rejecter temperature (T_3) are commonly fixed by the application. The objective is to get the highest increase in coefficient of performance (COP_{gain}) compared to the baseline cycle. Independent design parameters are the mass flow ratio ($K=m_6/m_2$) that relates the mass flow of the cooling cycle to the mass flow of the refrigerant cycle, and the pressure ratio of the wave rotor ($PR_W=p_3/p_2$).

Additional assumptions considered in the thermodynamic model are the following:

1. For comparison of baseline and enhanced cycles, the evaporator and condenser inlet temperatures are considered to be the same ($T_1=T_{1b}$ and $T_3=T_{3b}$).
2. Temperature difference across the heat rejecter is kept constant ($T_5-T_3=3$ K).
3. Pressure drop in heat rejecter, evaporator, and pipes is neglected.
4. The condenser and evaporator outlet states are fully saturated.
5. Same polytrophic compressor efficiency is used for baseline and enhanced cycles. Its value of 0.72 is obtained by assuming an isentropic efficiency of 0.7 for a compressor with a pressure ratio of 2.
6. The superheated vapor is considered as an ideal gas ($\gamma=1.33$).
7. One-dimensional gasdynamic shock wave equations are used to calculate the flow properties across the moving normal shock wave. Reflected shock waves are not considered.
8. The hydraulic efficiency of the pump is 0.9.

Figure 8 shows the relative COP_{gain} versus the evaporator temperature (T_1) for different mass flow ratios. By increasing evaporator temperature T_1, the COP of the wave-rotor-enhanced cycle is increased relative to the COP of the baseline cycle. This trend is seen until the compressor pressure ratio in the enhanced cycle

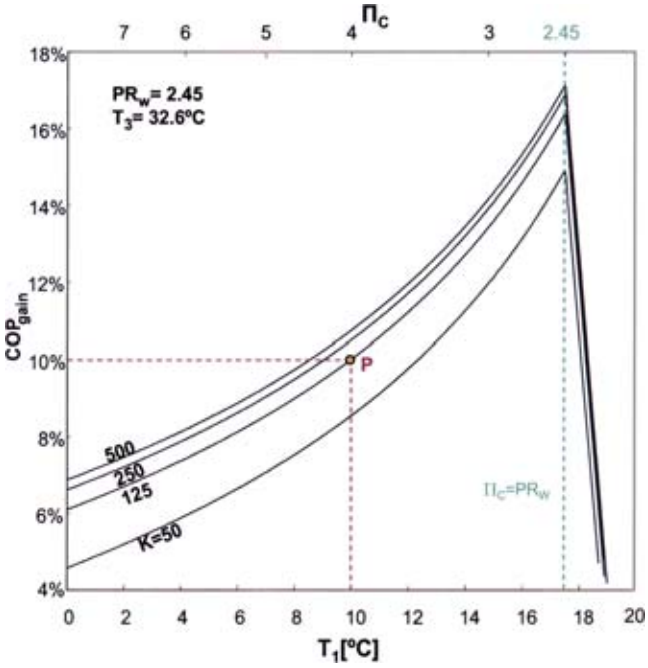

Fig. 8 Relative COP increase versus evaporation temperature for different mass flow ratios

($\Pi_c=p_2/p_1$) is reduced to a value that is equal to the wave rotor pressure ratio ($\Pi_c=PR_W$). After that the relative COP_{gain} drops dramatically.

Figure 9 represents the relative COP_{gain} versus mass flow ratio for different evaporator temperatures, like a side view of Fig. 8. It shows only the increasing branches of Fig. 8 up to an evaporation temperature where the pressure ratio of the turbocompressor is reduced to the value of the wave rotor pressure ratio. Increasing the mass flow ratio above 200 appears as ineffective according to Fig. 9.

Figure 10 shows the effect of the wave rotor pressure ratio

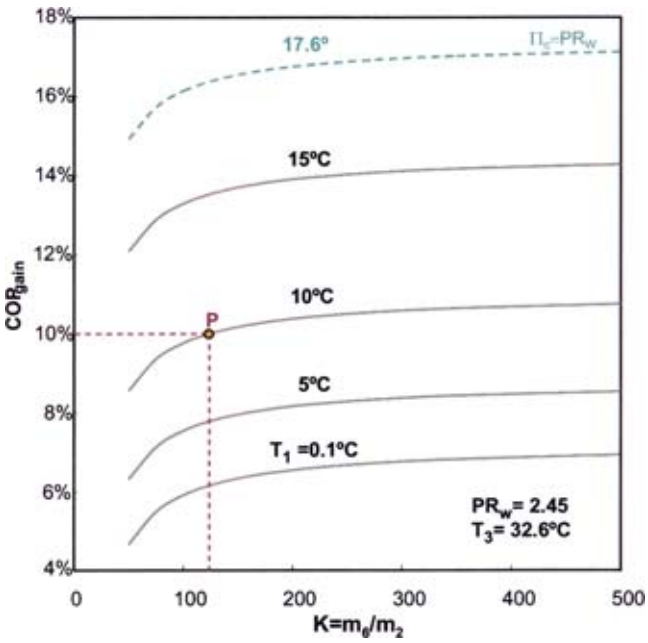

Fig. 9 Relative COP increase versus mass flow ratio for different evaporation temperatures

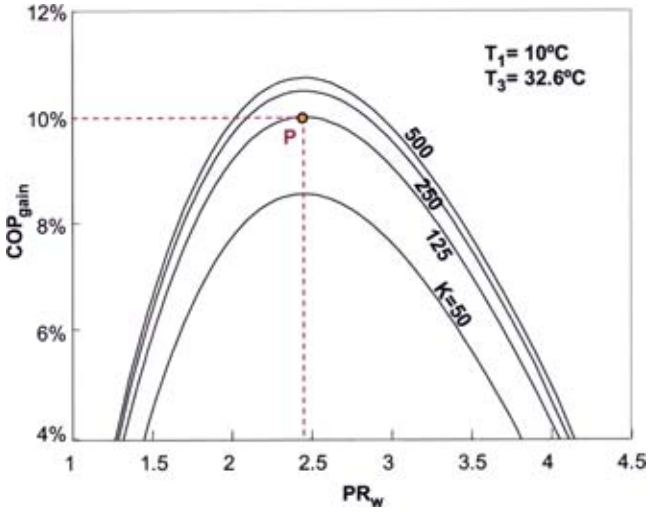

Fig. 10 Relative COP increase versus the wave rotor pressure ratio for different mass flow ratios

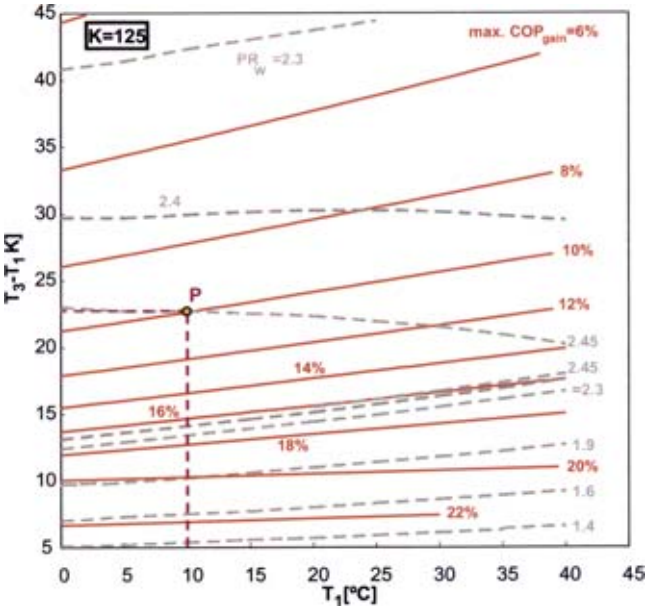

Fig. 12 Performance map: maximum performance increase and optimum wave rotor pressure ratios

(PR_W) on the relative COP_{gain} for different mass flow ratios. Each curve has a maximum point that indicates the best choice of wave rotor pressure ratio for the given system specifications. The location of this point depends on several parameters including the hydraulic efficiency of the pump, compressor polytropic efficiency, evaporator temperature, and temperature lift (T_3-T_1), but not the mass flow ratio. One common characteristic shown in Figs. 8, 9, and 10 is that a continued increase of the independent value does not always increase the COP_{gain}. While Fig. 10 shows this effect for the wave rotor pressure ratio, Fig. 8 reveals a growing gradient of COP_{gain} up to the point where further increase of evaporator temperature actually reduces COP_{gain}. A similar trend can be seen in Fig. 9 where the curves have an asymptotic behavior for increased mass flow ratio.

Figure 11 shows the heat rejecter temperature (T_3) versus evaporator temperature for different wave rotor pressure ratios and a constant relative COP_{gain} of 10%. The figure indicates that there are several options for the wave rotor pressure ratio to obtain a certain relative COP_{gain}. However, only the optimum pressure ratio of 2.45 yields the highest temperature lift.

Figure 12 is a performance map of the enhanced cycle. Each point on this plot shows the maximum COP_{gain} that can be obtained by the optimum choice of PR_W for a given evaporator temperature and a temperature lift. The constant PR_W lines indicate the optimum PR_W that yields the highest possible COP_{gain} indicated by constant max. COP_{gain} lines.

In this performance plot of optimized points, an arbitrary optimum point P is marked. It is used to show the connection between all the performance graphs. However, it is the only optimum point in the performance plots of Figs. 8–11. All other points of these plots are not found in Fig. 12 because they show a smaller COP_{gain} than the points in Fig. 12.

The trend found in Fig. 8 was that for a given heat rejecter temperature (T_3) and PR_W, an increase of the evaporator temperature results in a higher COP_{gain}. Such an effect can also be seen in the performance map of the optimized points (Fig. 12) by moving point P to the right along constant PR_W line of 2.45. However, for smaller temperature lifts below about 15 K (above max. COP_{gain} of about 16%) this effect is reversed such that the max. COP_{gain} decreases with increasing evaporator temperature.

Figure 10 showed that for a given mass flow ratio and a combination of evaporation and heat rejecter temperatures there is a maximum COP_{gain}. Since the point P is at the maximum of the dome it also appears in Fig. 12.

The following results can be obtained from the performance map of optimized points:

1. As lower the temperature lift, as higher the relative max. COP_{gain} of the enhanced cycle.
2. The maximum optimum PR_W for a condensing 3-port wave rotor is about 2.51.
3. While below a temperature lift of approximately 18 K the optimum PR_W increases with the temperature lift, decreases slightly for higher temperature lifts. This trend shows a rapidly decreasing gradient with increasing temperature lift.
4. Slope of constant COP_{gain} lines increases as the temperature lift increases, showing that an increase of evaporation tem-

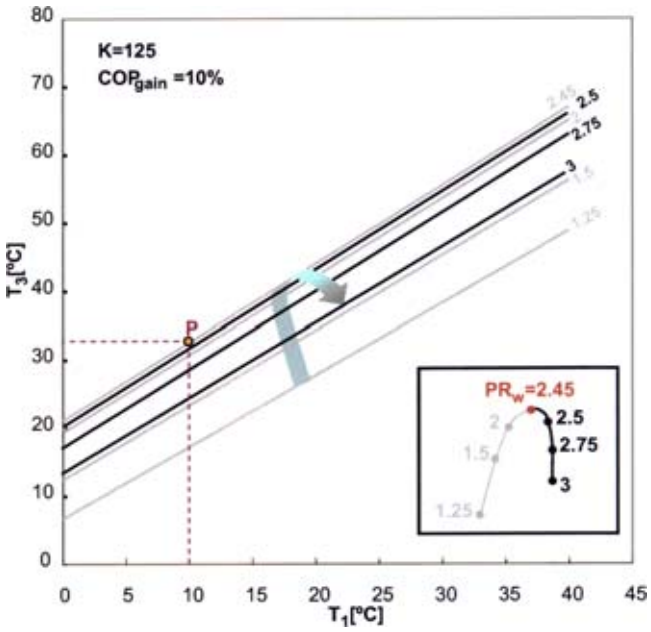

Fig. 11 Heat rejecter temperature versus evaporator temperature for different wave rotor pressure ratios

perature is even more beneficial for the enhanced cycle, especially for greater temperature lifts as it is already the case for the R718 baseline cycle.

Summary

The potential of using wave devices in R718 refrigeration cycles is demonstrated. Advantages of cycles working with water as a refrigerant (R718) and challenges involved with designing them are mentioned. To enhance the turbocompression and improve the efficiency of such cycles, the novel concept of using a 3-port condensing wave rotor in a R718 compression refrigeration cycle is investigated. The condensing wave rotor employs pressurized water to pressurize, desuperheat, and condense the superheated vapor coming from the compressor—all in one dynamic process. The $p-h$ and $T-s$ diagrams of the external process and the wave and phase-change diagram of the internal process are discussed. Flash evaporation, shock wave compression, desuperheating, and condensation phenomena inside the wave rotor channels are described. A computer code based on a thermodynamic model was generated to evaluate the performance improvement of R718 cycles enhanced with 3-port condensing wave rotors. The effect of some of the key parameters on the relative increase of the coefficient of performance of the wave-rotor-enhanced cycle is shown. Finally a performance map showing the optimized points of the enhanced cycle is presented. The presented results show an improvement of the COP of up to 22% by using the 3-port condensing wave rotor. Beside this, the condensing wave rotor allows lower compressor pressure ratios for the same temperature lift or increases the temperature lift without changing the compressor. This wave rotor is a simple drum easy to manufacture, rotating at relatively low speed. Since it performs compression, desuperheating, and condensation in one compact device it can reduce the size and cost of modern state-of-the-art R718-chillers that now employ high-tech multistage compressors, intercooler, and relative bulky condensers.

References

[1] Weber, H. E., 1995, *Shock Wave Engine Design*, John Wiley and Sons, New York.

[2] Weber, H. E., 1986, "Shock-Expansion Wave Engines: New Directions for Power Production," ASME Paper 86-GT-62.

[3] Akbari, P., Kharazi, A. A., and Müller, N., 2003, "Utilizing Wave Rotor Technology to Enhance the Turbocompression in Power and Refrigeration Cycles," 2003 International Mechanical Engineering Conference, ASME Paper IMECE2003-44222.

[4] Taussig, R. T., and Hertzberg, A., 1984, "Wave Rotors for Turbomachinery," Winter Annual Meeting of the ASME, edited by Sladky, J. F., Machinery for Direct Fluid-Fluid Energy Exchange, AD-07, pp. 1–7.

[5] Shreeve, R. P., and Mathur, A., 1985, Proceeding ONR/NAVAIR Wave Rotor Research and Technology Workshop, Report NPS-67-85-008, Naval Postgraduate School, Monterey, CA.

[6] Paxson, D. E., 1995, "Comparison Between Numerically Modeled and Experimentally Measured Wave-Rotor Loss Mechanism," J. Propul. Power, **11**, pp. 908–914; see also NASA TM-106279.

[7] Paxson, D. E., 1996, "Numerical Simulation of Dynamic Wave Rotor Performance," J. Propul. Power, **12**, pp. 949–957.

[8] Wilson, J., and Paxson, D. E., 1996, "Wave Rotor Optimization for Gas Turbine Topping Cycles," J. Propul. Power, **12**, No. 4, pp. 778–785; see also SAE Paper 951411, 1995, and NASA TM 106951.

[9] Welch, G. E., Jones, S. M., and Paxson, D. E., 1997, "Wave Rotor-Enhanced Gas Turbine Engines," J. Eng. Gas Turbines Power, **119**, No. 2, pp. 469–477.

[10] Welch, G. E., 1997, "Macroscopic Balance Model for Wave Rotors," J. Propul. Power, **13**, No. 4, pp. 508–516.

[11] Welch, G. E., 1997, "Two-Dimensional Computational Model for Wave Rotor Flow Dynamics," J. Eng. Gas Turbines Power, **119**, No. 4, pp. 978–985.

[12] Wilson, J., 1998, "An Experimental Determination of Loses in a Three-Port Wave Rotor," J. Eng. Gas Turbines Power, **120**, pp. 833–842.

[13] Paxson, D. E., and Nalim, M. R., 1999, "Modified Through-Flow Wave-Rotor Cycle With Combustor Bypass Ducts," J. Propul. Power, **15**, No. 3, pp. 462–467.

[14] Welch, G. E., 2000, "Overview of Wave-Rotor Technology for Gas Turbine Engine Topping Cycles," Novel Aero Propulsion Systems International Symposium, The Institution of Mechanical Engineers, pp. 2–17.

[15] Fatsis, A., and Ribaud, Y., 1999, "Thermodynamic Analysis of Gas Turbines Topped With Wave Rotors," Aerospace Sci. Technol., **3**, No. 5, pp. 293–299.

[16] Jones, S. M., and Welch, G. E., 1996, "Performance Benefits for Wave Rotor-Topped Gas Turbine Engines," ASME Paper 96-GT-075.

[17] Akbari, P., and Müller, N., 2003, "Performance Improvement of Small Gas Turbines Through Use of Wave Rotor Topping Cycles," 2003 International ASME/IGTI Turbo Exposition, ASME Paper GT2003-38772.

[18] Doerfler, P. K., 1975, "Comprex Supercharging of Vehicle Diesel Engines," SAE Paper 750335.

[19] Doerfler, P. K., 1975, "Comprex Supercharging of Vehicle Diesel Engines," SAE Paper 750335.

[20] Eisele, E., Hiereth, H., and Polz, H., 1975, "Experience With Comprex Pressure Wave Supercharger on the High-Speed Passenger Car Diesel Engine," SAE Paper 750334.

[21] Kollbrunner, T. A., 1980, "Comprex® Supercharging for Passenger Diesel Car Engines," SAE Paper 800884.

[22] Gyarmathy, G., 1983, "How Does the Comprex® Pressure-Wave Supercharger Work," SAE Paper 830234.

[23] Schneider, G., 1986, "Comprex® Pressure Wave Supercharger in An Opel Senator With 2.3 Liter Diesel Engine," Brown Boveri Rev., **73**, No. 10, pp. 563–565.

[24] Zehnder, G., Mayer, A., and Mathews, L., 1989, "The Free Running Comprex®," SAE Paper 890452.

[25] Mayer, A., Oda, J., Kato, K., Haase, W., and Fried, R., 1989, "Extruded Ceramic—A New Technology for the Comprex® Rotor," SAE Paper 890453.

[26] Amstutz, A., Pauli, E., and Mayer, A., 1990, "System Optimization With Comprex Supercharging and EGR Control of Diesel Engines," SAE Paper 905097.

[27] Kentfield, J. A. C., 1998, "Wave Rotors and Highlights of Their Development," AIAA Paper 98-3248.

[28] Kentfield, J. A. C., 1993, *Nonsteady, One-Dimensional, Internal, Compressible Flows*, Oxford University Press, Oxford.

[29] Azoury, P. H., 1992, *Engineering Applications of Unsteady Fluid Flow*, Wiley, New York.

[30] Albring, P., 1994, "Water as Refrigerant in Refrigeration Plants With Mechanical Compression," New Applications of Natural Working Fluids in Refrigeration and Air Conditioning, IIR, Hannover, pp. 735–742.

[31] Albring, P., and Heinrich, G., 1996, "R718 Heat Pumps: Applications for Natural Refrigerants," IIR, Aarhus, pp. 553–558.

[32] Albring, P., and Heinrich, G., 1998, "Turbo Chiller With Water as Refrigerant," Natural Working Fluids '98, IIR, Oslo, pp. 93–103.

[33] Heinrich, G., Janik, A., and Albring, P., 1991, "Alternative Kaleprozesse mit R718 (H20)," Luft- und Kaltetechnik, **27**, p. 3.

[34] Albring, P., and Müller, N., 1995, "Turboverdichter für Wasser als Kältemittel" (Turbo-compressors for Water as a Refrigerant) in Faragallah, W., Surek, D., "Beiträge zu Fluidenergiemaschinen," Sulzbach, Band **2**, pp. 16–22.

[35] Müller, N., 2002, "Turbo Chillers Using Water as a Refrigerant," ASME PID Newsletter, p. 3.

[36] Müller, N., 2001, "Design of Compressor Impellers for Water as a Refrigerant," ASHRAE Trans., **107**, pp. 214–222.

[37] Saury, D., Harmand, S., and Siroux, M., 2002, "Experimental Study of Flash Evaporation of Water Film," Int. J. Heat Mass Transfer, **45**, pp. 3447–3457.

[38] Miyatake, O., Murakami, K., and Kawata, Y., 1973, "Fundamental Experiments With Flash Evaporation," Heat Transfer-Jpn. Res., **2**, pp. 89–100.